Phytopathology Research

RESEARCH

Open Access

The structural diversity of xanthomonadin aryl polyenes and functional analysis of the genes required for their synthesis by *Xanthomonas* phytopathogens

Wen-Da Hu[1†], Bing Chen[2†], Zhelin Zheng[1†], Xueqiang Cao[1], Kai Song[1], Alan Robert Poplawsky[3] and Ya-Wen He[1*]

Abstract

Xanthomonas is a genus of plant-associated Gram-negative bacteria which infect more than 400 plant species. A characteristic feature of *Xanthomonas* bacteria is the production of yellow membrane-bound pigments called xanthomonadins. Xanthomonadins are phospholipid-like bio-macromolecules located at the outer membrane. The chemical structure and biosynthetic mechanism of xanthomonadin production remain to be fully elucidated. In this study, a total of 24 *Xanthomonas* strains from five different species were collected for methylated ester of aryl polyene (MEAP) preparation. High-Performance Liquid Chromatography (HPLC) and Quadrupole Time-of-Flight Mass Spectrometry (Q-TOF–MS) analysis identified three dominant MEAPs, methylated di-brominated MEAP-1, di-brominated MEAP-2, and mono-brominated MEAP-3. MEAP-1 corresponded to the previously reported aryl polyene in *Xanthomonas juglandis* XJ103. The 24 *Xanthomonas* strains could be grouped into three categories based on their MEAP profiles. Further, bacterial ooze was collected from *X. oryzae* pv. *oryzae* (*Xoo*)-infected rice leaves and MEAP was prepared. The dominant MEAP in the *Xoo* ooze was MEAP-2. This is the first demonstration of *in-planta* MEAP production during plant infection of any *Xanthomonas* pathogen. In addition, a *xan* biosynthetic cluster, which is responsible for xanthomonadin biosynthesis, and the roles of the individual *xan* genes in MEAP biosynthesis were studied via deletion and subsequent complementation analysis. HPLC and Q-TOF–MS analysis identified the essential genes for MEAP biosynthesis, as well as the genes associated with methylation and bromination. These results provide new insights into the structural diversity of *Xanthomonas* MEAPs and xanthomonadin biosynthetic mechanisms.

Keywords *Xanthomonas*, Xanthomonadin, Aryl polyene, Bromination, Biosynthesis

[†]Wen-Da Hu, Bing Chen, Zhelin Zheng have contributed equally to this work.

*Correspondence:
Ya-Wen He
yawenhe@sjtu.edu.cn
Full list of author information is available at the end of the article

Background

Members of the *Xanthomonas* genus are plant-associated, Gram-negative bacteria which infect at least 400 different plant species, including the economically important crops of rice, wheat, oil rape, cabbage, orange, and banana (Leyns et al. 1984; He and Zhang 2008; An et al. 2020). Among them, *Xanthomonas campestris* pv. *campestris* (*Xcc*) causes black rot, one of the most important diseases of crucifers worldwide (Williams 1980; Vicente and Holub 2013). *X. oryzae* pv. *oryzae* (*Xoo*) and *X. oryzae* pv. *oryzicola* (*Xoc*) are respectively the causal agents of bacterial blight and bacterial leaf streak, two important diseases affecting worldwide rice production (Niño-Liu et al. 2006). X. *citri* pv. *citri* (*Xcci*) causes Asiatic citrus bacterial canker (Osdaghi, 2023), and *X. albilineans* (*Xal*) causes leaf scald, a lethal disease of sugarcane (Pieretti et al. 2015). The diverse array of *Xanthomonas* phytopathogens are continuing threats to worldwide agriculture (Vicente and Holub 2013).

A characteristic feature of *Xanthomonas* bacteria is the production of yellow membrane-bound pigments, referred to as xanthomonadins. Xanthomonadins are used as chemotaxonomic and diagnostic markers of the genus *Xanthomonas*. The methyl or isobutyl esters of xanthomonadin from *X. juglandis* strain XJ103 (re-classified to *X. aboricola* pv. *juglandis*) were first shown to be mixtures of unique, brominated aryl octanes (Andrewes et al. 1976). Among them, the isobutyl ester of aryl polyene I was chemically characterized as 17-(4-bromo-3-methoxyphenyl)-17-bromoheptadeca-2,4,6,8,10,12,14,16-octaenoate. Further studies demonstrated that the aryl polyenes from different *Xanthomonas* species differ in bromination and methylation patterns (Starr et al. 1977). Aririatu and Kester (1985) separated the pigments of *X. juglandis* ATCC 11329 on silica gel columns and identified two major esters, types 1 and 2. Further analysis demonstrated the presence of phosphate, glycerol, and sorbitol in ester 1, and phosphate and glycerol in ester 2. Hence, the authors proposed a putative phospholipid-like chemical structure for xanthomonadin. This was further supported by the finding that xanthomonadins could be extracted and separated by methods optimized for phosphatidylcholine extraction and separation (Moser et al. 2014). However, the full chemical structure of xanthomonadins remains to be elucidated.

The polyene structure similarities between carotenoids and xanthomonadins have led to considerable research interest in the biological roles of xanthomonadins. Current evidence suggests that xanthomonadin pigments may play a role in establishing or maintaining adaptation and virulence in *Xanthomonas* (He et al. 2020). Specifically with *Xcc*, the pathogen arrives on the leaf surface, expands its populations, and then moves to the hydathodes or wounds to infect the host plant. After this epiphytic phase and infection, the pathogen expands within the host plant and causes disease. Xanthomonadins enable *Xanthomonas* survival on plant leaf surfaces by protecting against photobiological damage (Poplawsky et al. 2000). These pigments also confer antioxidant activities which enable *Xanthomonas* survival and infection inside host plants (Rajagopal et al. 1997; He et al. 2011); however, the *in planta* biological roles of xanthomonadins require further elucidation.

Several studies have mapped the xanthomonadin biosynthetic genes to an ~ 18.2 kb *xan* (previously called *pig*) gene cluster in *Xcc* (Poplawsky et al. 1993; Goel et al. 2002; Cao et al. 2018). Among the *xan* genes, *xanB2* encodes a unique bifunctional chorismatase that hydrolyses chorismate to produce 3-hydroxybenzoic acid (3-HBA) and 4-hydroxybenzoic acid; 3-HBA is then further used for xanthomonadin biosynthesis (Zhou et al. 2013). The genes *xanA2* and *xanC* are responsible for the synthesis of 3-hydroxybenzoic acid-S-acyl carrier protein (3-HBA-S-ACP), both involved in xanthomonadin biosynthesis (Cao et al. 2018). Together with bioinformatic analysis, a four-step biosynthetic pathway was proposed (He et al. 2020). To further verify the proposed pathway, we generated a series of mutants corresponding to the *xan* genes in *Xcc* strain XC1. Xanthomonadin production and mutant colony color analysis previously identified the key genes involved in the xanthomonadin biosynthetic pathway (Cao et al. 2018). However, this analysis failed to identify the genes required for the structural modifications of xanthomonadin.

In this study, we have improved the methods for isolation of the xanthomonadin methyl ester aryl polyene (MEAPs), and established an Ultra-High Performance Liquid Chromatography Coupled with Quadrupole Time-of-Flight Mass Spectrometry (UPLC-Q-TOF–MS)-based method for MEAP structural characterization. With these improved methods, MEAP analysis was conducted on 24 *Xanthomonas* strains, and the roles of *xan* genes in *Xcc* MEAP biosynthesis were analyzed. Our goal was to answer the following three questions: (1) What is the structural diversity of aryl polyenes in *Xanthomonas*? (2) What are the roles of each *xan* gene in the biosynthesis of aryl polyenes in *Xcc*? (3) What is the chemical structure of the aryl polyene produced *in planta* during *Xanthomonas* infection?

Results

Growth and xanthomonadin yields of 24 *Xanthomonas* strains

We first studied 24 *Xanthomonas* strains, including 12 *Xcc* strains, 5 *Xoo* strains, 3 *Xoc* strains, 2 *Xal* strains,

and 2 *Xcci* strains (Table 1). Culture media YEBB, NYGB, LBB, and XYSB were used to produce 48-h growth curves, which were analyzed with a Bioscreen C Automated Growth Curve Analyzer. NYGB was optimal for growth for *Xcc* strains XC1, CN01, CN05, and CN15, while XYSB was optimal for growth for *Xcc* strain ATCC33913 (Fig. 1a). The other *Xcc* strains preferred YEBB medium for optimal growth. All 5 *Xoo* strains, 3 *Xoc* strains, and 2 *Xal* strains showed optimal growth in the YEBB medium. The two Xcc*i* strains grew well in all four media, displaying only minimal differences in OD_{600} readings at later stages of growth (Fig. 1a).

The xanthomonadin yields of each strain were determined in each of the four types of media after 48 h of growth (Fig. 1b). *Xcc* strains had the highest xanthomonadin yields, followed by *Xoo* and *Xoc*, whereas *Xal* strains had the lowest xanthomonadin production. Among the 12 *Xcc* strains, XC1, ATCC33913, CN01, CN05, and CN11 produced the highest levels of xanthomonadins in NYGB medium. *Xcc* strains CN04 and CN18 produced similarly high levels of xanthomonadins in the three media, YEBB, NYGB, and LBB, whereas CN17 preferred YEBB and NYGB media for maximum xanthomonadin production. Of all the media tested, YEBB was optimal for growth and xanthomonadin production with the greatest number of *Xanthomonas* strains. Therefore, YEBB was selected as the growth medium for all the *Xanthomonas* strains for the xanthomonadin MEAP pattern assays.

HPLC and UPLC-Q-TOF–MS analysis of the MEAPs of 24 *Xanthomonas* strains

Strains were cultured in YEBB medium for 48 h, and cell pellets were collected for xanthomonadin extraction and MEAP preparation. HPLC analysis of the purified MEAPs identified three dominant variants, MEAP-1, MEAP-2, and MEAP-3, with elution times of 47.6, 37.6, and 31.7 min, respectively (Fig. 2). Based on MEAP patterns, the 12 *Xcc* strains could be divided into two groups. Group I included XC1, CN01, CN04, CN07, CN11, CN17, and CN18, which produced mostly MEAP-1 (Fig. 2; Table 2). Group II contains 8004, ATCC33913, CN05, CN09, and CN15 produced mostly MEAP-2, which was also the case with the *Xoo* and both *Xal* strains. In contrast, with the three *Xoc* strains, MEAP-1 was dominant, like *Xcc* Group I strains. Interestingly, the two *Xcci* strains produced significant quantities of

Table 1 *Xanthomonas* parent strains used in this study

Strains	Plant Disease	Source
X. campestris pv. *campestris* XC1	Black rot of crucifers	Lab stock
X. campestris pv. *campestris* 8004	Black rot of crucifers	Lab stock
X. campestris pv. *campestris* ATCC33913	Black rot of crucifers	Lab stock
X. campestris pv. *campestris* CN01	Black rot of crucifers	Heilongjiang Province, China
X. campestris pv. *campestris* CN04	Black rot of crucifers	Inner mongolia Autonomous Region, China
X. campestris pv. *campestris* CN05	Black rot of crucifers	Beijing, China
X. campestris pv. *campestris* CN07	Black rot of crucifers	Tianjin, China
X. campestris pv. *campestris* CN09	Black rot of crucifers	Shaanxi Province, China
X. campestris pv. *campestris* CN11	Black rot of crucifers	Henan Province, China
X. campestris pv. *campestris* CN15	Black rot of crucifers	Guangxi Autonomous Region, China
X. campestris pv. *campestris* CN17	Black rot of crucifers	Guangxi Autonomous Region, China
X. campestris pv. *campestris* CN18	Black rot of crucifers	Guangxi Autonomous Region, China
X. oryzae pv. *oryzae* PXO99^{A}	Bacterial blight of rice	Lab stock
X. oryzae pv. *oryzae* KACC 10331	Bacterial blight of rice	Korean Collection for Type Cultures (KCTC)
X. oryzae pv. *oryzae* X235	Bacterial blight of rice	Xiamen, Fujian Province of China
X. oryzae pv. *oryzae* JL1	Bacterial blight of rice	Jilin Province of China
X. oryzae pv. *oryzae* YN04-1	Bacterial blight of rice	Yunnan Province of China
X. oryzae pv. *oryzicola* YNB01-3	Bacterial leaf streak of rice	Yunnan Province of
X. oryzae pv. *oryzicola* HNB8-47	Bacterial leaf streak of rice	Hainan Province of China
X. oryzae pv. *oryzicola* HANB1-19	Bacterial leaf streak of rice	Hainan Province of China
X. albilineans FJ1	Leaf scald of sugarcane	Fujian Agriculture and Forestry University
X. albilineans CN24	Leaf scald of sugarcane	Fujian Agriculture and Forestry University
X. citri pv. *citri* 49	Citrus canker	Hubei Province of China
X. citri pv. *citri* 29–1	Citrus canker	Hubei Province of China

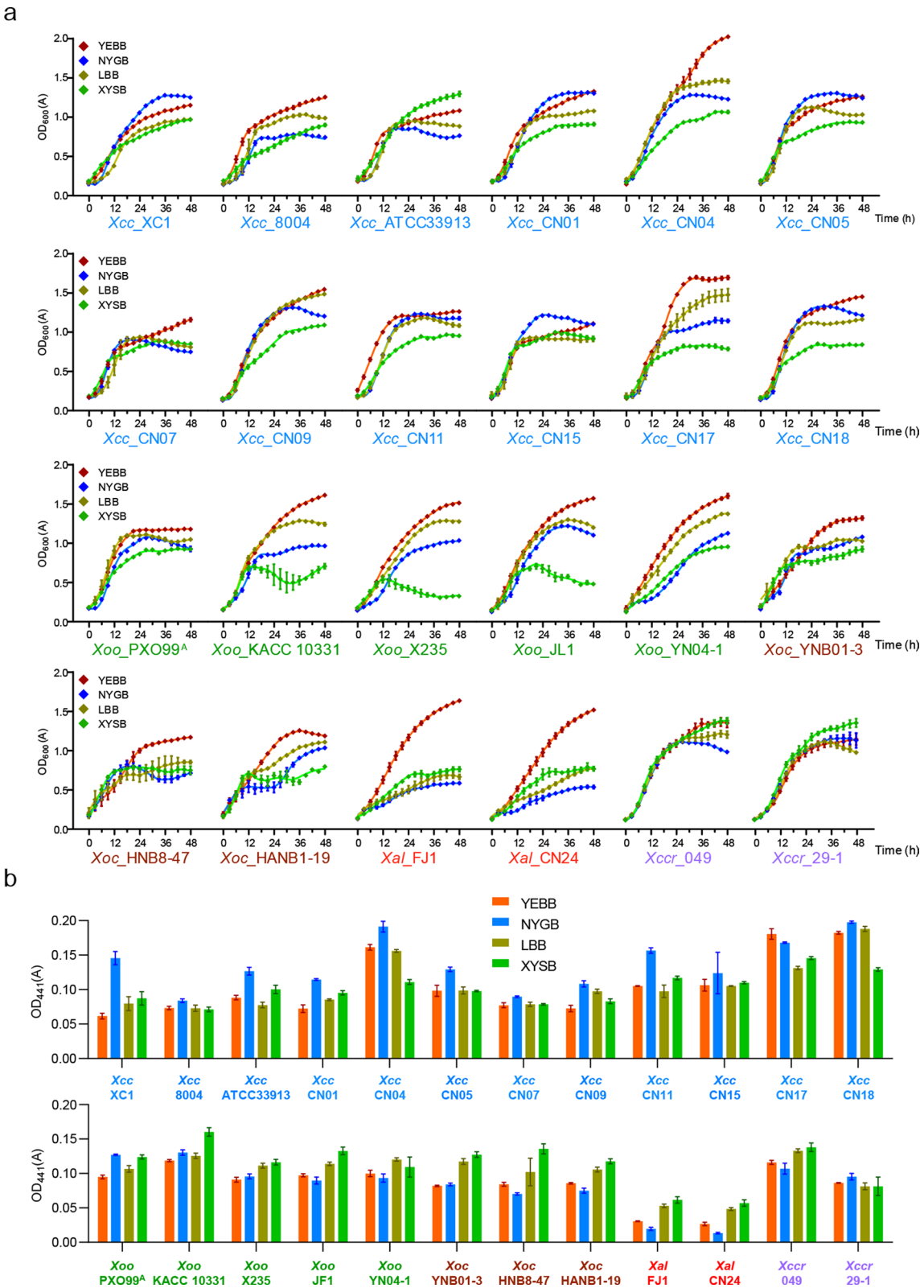

Fig. 1 Growth curves and xanthomonadin yields of 24 *Xanthomonas* strains. **a** Growth curves in 4 types of liquid media: YEBB, NYGB, LBB, and XYSB. OD_{600} was measured every 15 min using a Bioscreen C Automated Growth Curve Analyzer. **b** Xanthomonadin yield in four types of liquid media. Three independent experiments were conducted, and averages and standard deviations are shown

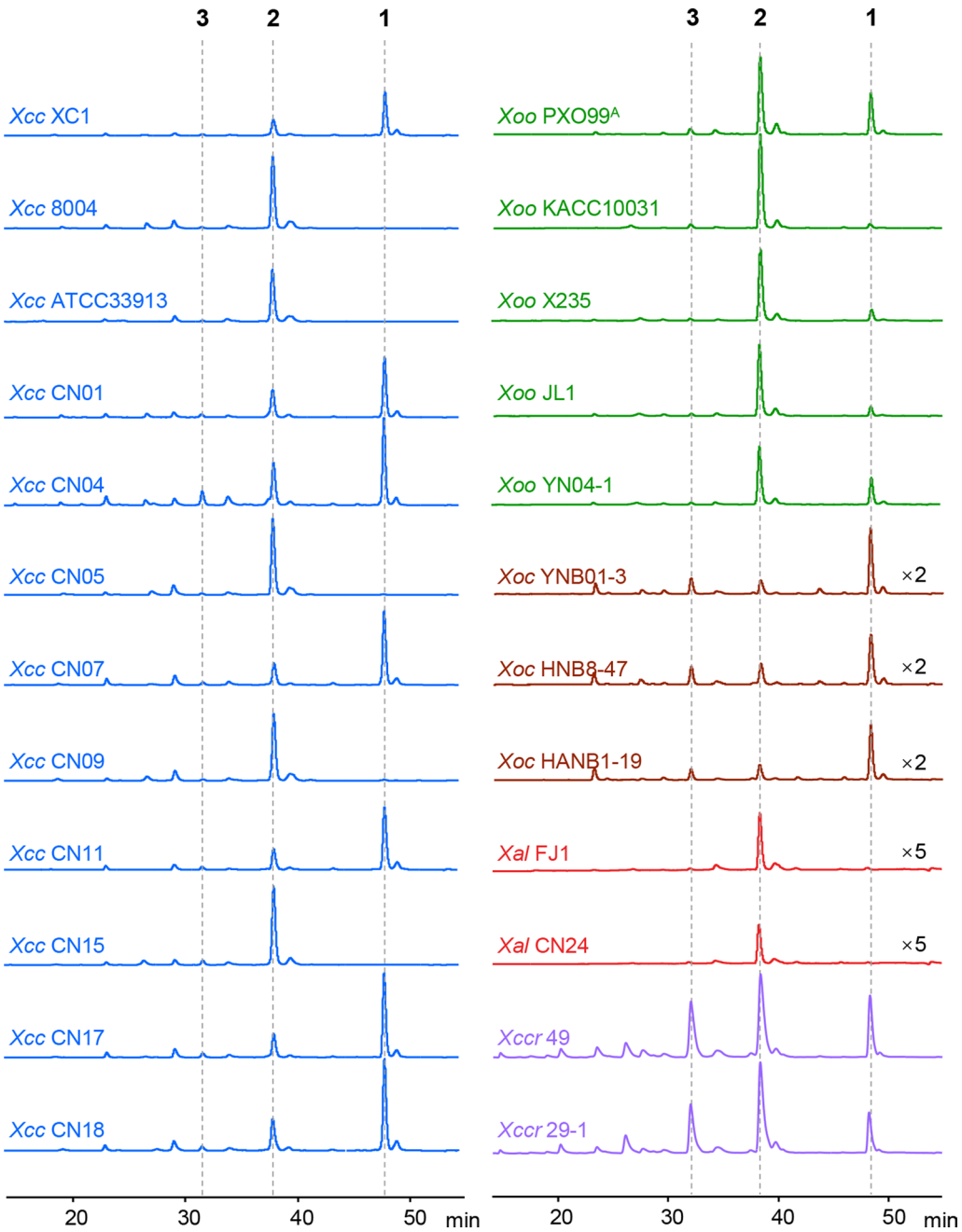

Fig. 2 HPLC analysis of methyl esters of aryl polyene (MEAPs) in 24 *Xanthomonas* strains. *Xcc*: *Xanthomonas campestris* pv. *campestris*; *Xoo*: *Xanthomonas oryzae* pv. *oryzae*; *Xoc*: *Xanthomonas oryzae* pv. *oryzicola*; *Xal*: *Xanthomonas albilineans*; *Xcci*: *Xanthomonas citri* pv. *citri*. × 2 or × 5: MEAPs from *Xoc* and *Xal* were concentrated 2 times and 5 times, respectively, before being subjected to HPLC analysis

all three MEAPs and were therefore placed in Group III (Table 2).

The wavelengths of maximum absorbance for MEAPs -1, -2, and -3 are 445, 445, and 442 nm, respectively (Fig. 3a). High-resolution Q-TOF–MS analysis identified bromine in all three MEAPs. MEAP-1 had a relative abundance ratio of 1:2:1 for the observed productions at *m/z* 531.0178, 533.0161, and 535.0151, indicating that MEAP-1 contains two bromines (Fig. 3b). The observed *m/z* 531.0178, 533.0161, and 535.0151 in MEAP-1 MS spectra suggested a molecular formula of $C_{25}H_{24}Br_2O_3$ ($[M+H]^+$ *m/z* 531.0165, 533.0146, and 535.0151). The high-resolution MS data of MEAP-1 matched that of the previously identified aryl polyene I

Table 2 Three categories of *Xanthomonas* strains (I, II, and III) based on methyl ester of aryl polyene (MEAP) profiles. MEAP-1: Di-brominated, methylated MEAP ($C_{25}H_{24}Br_2O_3$); MEAP-2: Di-brominated, unmethylated MEAP ($C_{24}H_{22}Br_2O_3$); MEAP-3: Mono-brominated, unmethylated MEAP ($C_{24}H_{23}BrO_3$)

Category	Dominant MEAP			*Xanthomonas* Strains	
	1	2	3		
I	+ + + + +	+	+	*Xcc* strains	XC1, CN01, CN04, CN07, CN11, CN17, CN18
				Xoc strains	YNB01-3, HNB8-47, HANB1-19
II	+	+ + + + +	+	*Xcc* strains	ATCC33913, 8004, CN05, CN09, CN15
				Xoo strains	PXO99^A, KACC10331, X235, JL1
				Xal strains	FJ1, CN24
III	+ +	+ + +	+ + +	*Xcci* strains	49, 29–1

[17-(4-bromo-3-methoxyphenyl)-17-bromo-heptadeca-2,4,6,8,10,12,14,16-octaenoate] from *X. aboricola* pv. *juglandis* XJ103 (Andrewes et al. 1976). Thus, MEAP-1 was structurally defined as a methyl ester of methylated di-brominated aryl polyene. The Q-TOF–MS data analysis suggested that MEAP-2 is structurally similar to MEAP-1 but lacks a methyl group, with a molecular formula of $C_{24}H_{22}Br_2O_3$ (Fig. 3c). MEAP-2 was therefore structurally defined as a methyl ester of di-brominated aryl polyene.

In MEAP-3, the relative abundance ratio of the observed *m/z* 439.0906 and *m/z* 441.0809 was 1:1, indicating that MEAP-3 contains one bromine (Fig. 3d). The observed *m/z* 439.0906 and *m/z* 441.0809 in the MEAP-3 MS analysis suggested a molecular formula of $C_{24}H_{23}BrO_3$ ($[M+H]^+$ *m/z* 439.0903 and 441.0886). These data suggest that MEAP-3 is a methyl ester of mono-brominated aryl polyene with two putative chemical structures (Fig. 3d).

Xoo produces MEAP-2 in rice leaf tissue

Xoo is a vascular pathogen that causes bacterial blight in rice. Granular dried *Xoo* ooze can sometimes be observed at the edges of *Xoo*-infected rice leaf blades. These oozes probably represent the *Xoo* population inside the rice leaf tissues (Hayward 1993). In this study, the *Xoo*-infected hybrid rice (Huazheyou-1) was found at Dongyang, Zhejiang, China. The *Xoo* strain (ZJ12) was isolated from the infected tissue, and dried *Xoo* oozes were manually collected from the leaves (Fig. 4a). Five mg aliquots of the oozes were used for MEAP preparation. HPLC analysis identified a dominant MEAP-2 in the *Xoo* ooze (Fig. 4b). This is further supported by the subsequent Q-TOF–MS analysis (Fig. 4b). Analysis of *Xoo* strain ZJ12 grown in YEBB medium (Fig. 4c) also determined that MEAP-2 was dominant, as was found with the other five *Xoo* strains (Fig. 4d). Thus, the MEAP profile in the *Xoo* ooze was very similar to the profiles of the causal strain grown in YEBB medium and also those of the other *Xoo* strains (Fig. 2).

Functional analysis of *xan* genes for MEAP biosynthesis in *Xcc* strains XC1 and 8004

All sequenced *Xcc*, *Xal*, and *Xcci* strains contain a single conserved *xan* cluster responsible for xanthomonadin biosynthesis. Although the *xan* genes in *Xoo* and *Xoc* are located at two distinct sites, they are nevertheless highly conserved among all *Xanthomonas* strains (Fig. 5). To explore the molecular mechanisms underlying the MEAP structural diversity among *Xanthomonas* strains, functional analysis of all of the *xan* genes for MEAP biosynthesis and modification was conducted with *Xcc* strains 8004 and XC1.

We first generated 36 deletion mutants, each corresponding to a single *xan* gene in *Xcc* strains 8004 and XC1, and then analyzed their growth and MEAP profiles. We found that single deletions of all these *xan* genes had no significant effect on bacterial growth (Additional file 1: Figure S1). However, deletions of *xanA2*, *xanB2*, *xanC*, *xanE*, *xanF*, *xanG*, *xanH*, *xanJ*, *xanK*, *xanL*, and *xanM* abolished MEAP biosynthesis in both strains (Fig. 6). The colonies of these mutant strains were white on YEBB agar medium (Table 3). These results indicated

(See figure on next page.)

Fig. 3 Spectrophotometry and Mass Spectrometry (MS) of the dominant MEAPs of *Xanthomonas* strains. **a** UV/vis absorption spectra of MEAP-1, -2, and -3. **b–d** UPLC-Q-TOF–MS analysis of MEAP-1, -2, and -3. All the aryl polyenes were analyzed using UPLC-Q-TOF–MS based on bromine isotopic distributions. Mass spectrometry was performed on an Agilent 1290 Infinity II UPLC system equipped with a 6545 Accurate Mass Q-TOF mass spectrometer. Spectra were recorded in positive mode from Atmospheric Pressure Chemical Ionization (APCI) source. Data were collected and analyzed via the Agilent MassHunter software package

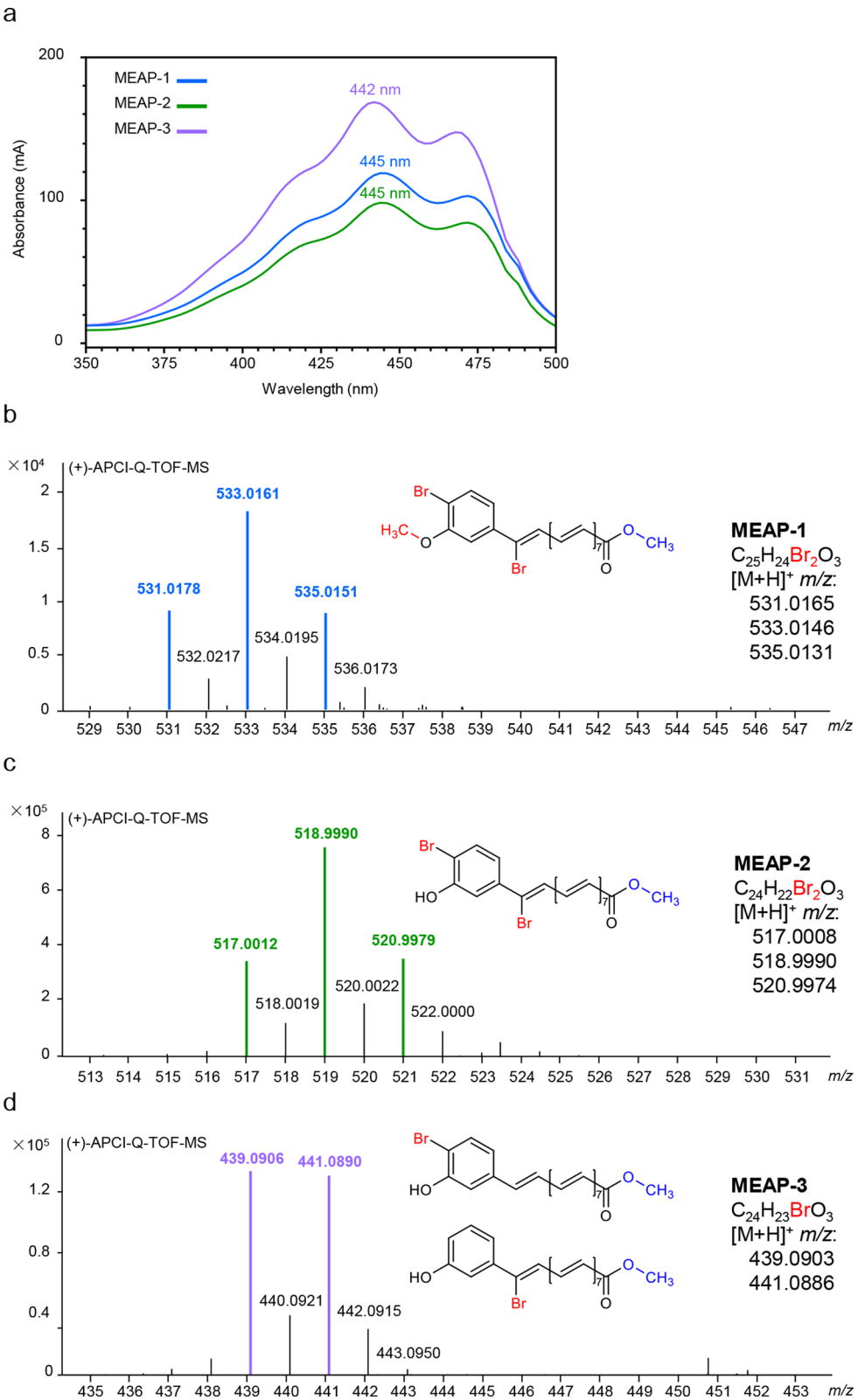

Fig. 3 (See legend on previous page.)

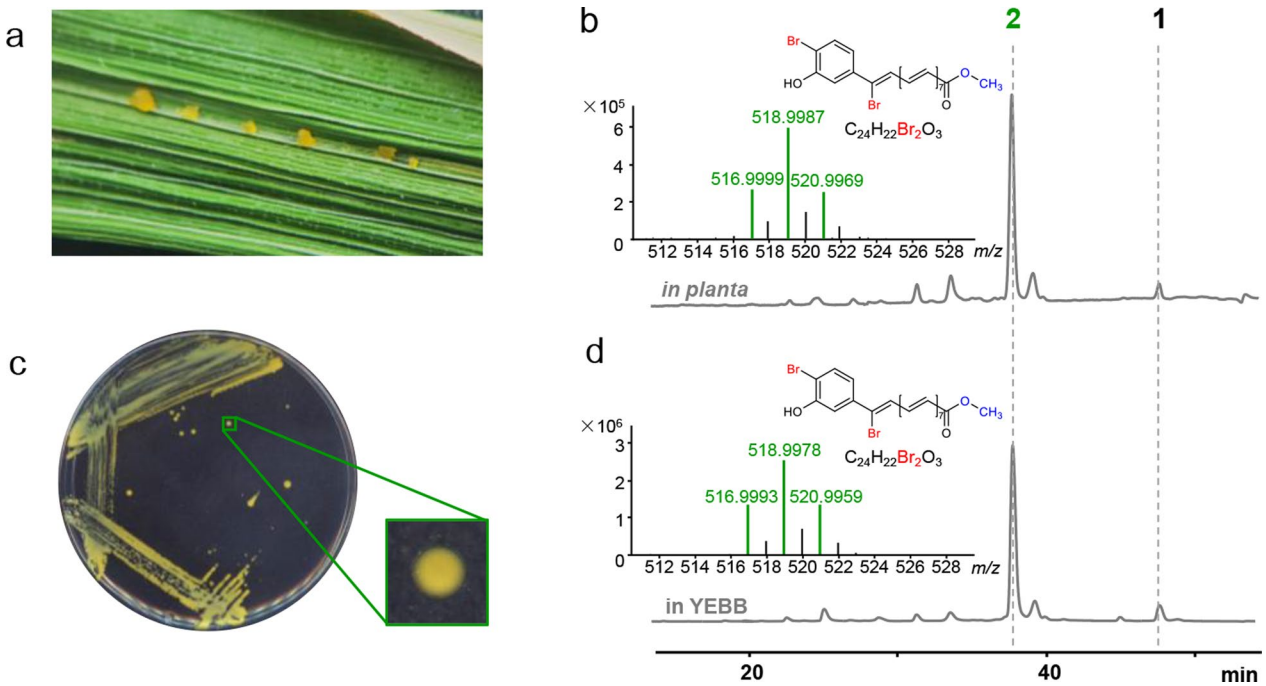

Fig. 4 HPLC and Q-TOF–MS analysis of the MEAPs from *Xoo* oozes of *Xoo*-infected rice (Huazheyou-1) and the causal strain *Xoo* ZJ-12. **a** Dried bacterial oozes on the surface of the *Xoo*-infected rice leaves in Dongyang, Zhejiang. **b** HPLC and Q-TOF–MS analysis of the dominant MEAP from *Xoo* oozes. **c** Identification of *Xoo* strain ZJ12 from the *Xoo*-infected rice leaves at Dongyang, Zhejiang. **d** HPLC and Q-TOF–MS analysis of the dominant MEAP prepared from the *Xoo* strain ZJ12 grown in liquid YEBB medium

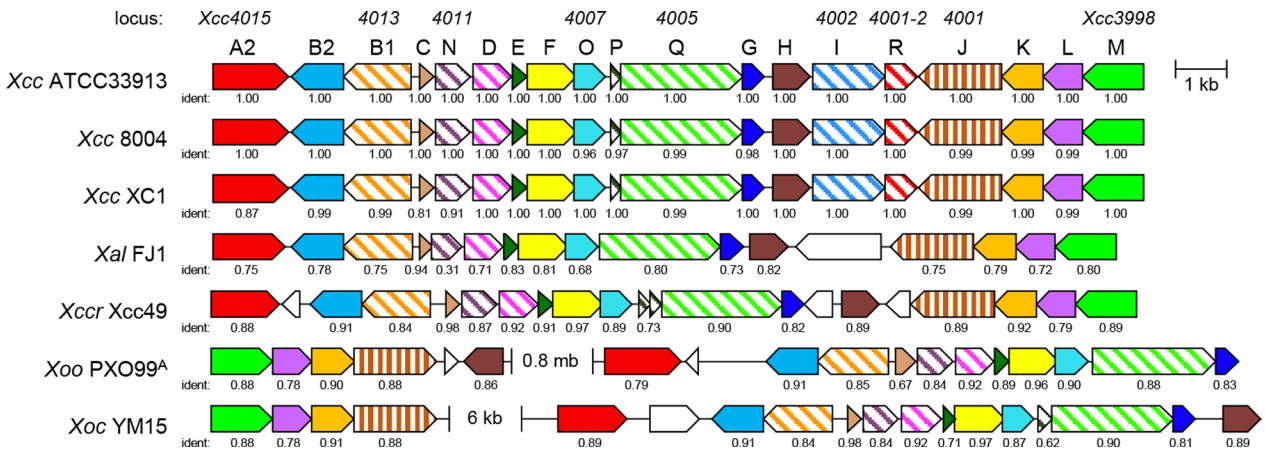

Fig. 5 The xanthomonadin biosynthetic gene cluster (*xan* cluster) of 6 *Xanthomonas* strains. *Xcc*: *Xanthomonas campestris* pv. *campestris*; *Xoo*: *Xanthomonas oryzae* pv. *oryzae*; *Xoc*: *Xanthomonas oryzae* pv. *oryzicola*; *Xal*: *Xanthomonas albilineans*; *Xcci*: *Xanthomonas citri* pv. *citri*. The numbers indicate the nucleotide sequence identity compared with *Xcc* strain ATCC33913

that these 11 genes are essential for MEAP or xanthomonadin biosynthesis.

Sequence analysis indicates that *xanB1* (*Xcc4013* in ATCC33913) encodes a 443-aa flavin-dependent halogenase. Deletion of *xanB1* had no significant effect on xanthomonadin yield, and the resultant mutant strain Δ*xanB1* was yellow on YEBB medium (Table 3). However, the dominant di-brominated MEAP-1 observed in strain XC1 and the dominant di-brominated MEAP-2 observed in strain 8004 were both missing, and each was replaced by the mono-brominated MEAP-3 as seen in the mutant strains XC1-Δ*xanB1* and 8004-Δ*xanB1* (Fig. 6). These results suggest that *xanB1* is responsible for MEAP bromination.

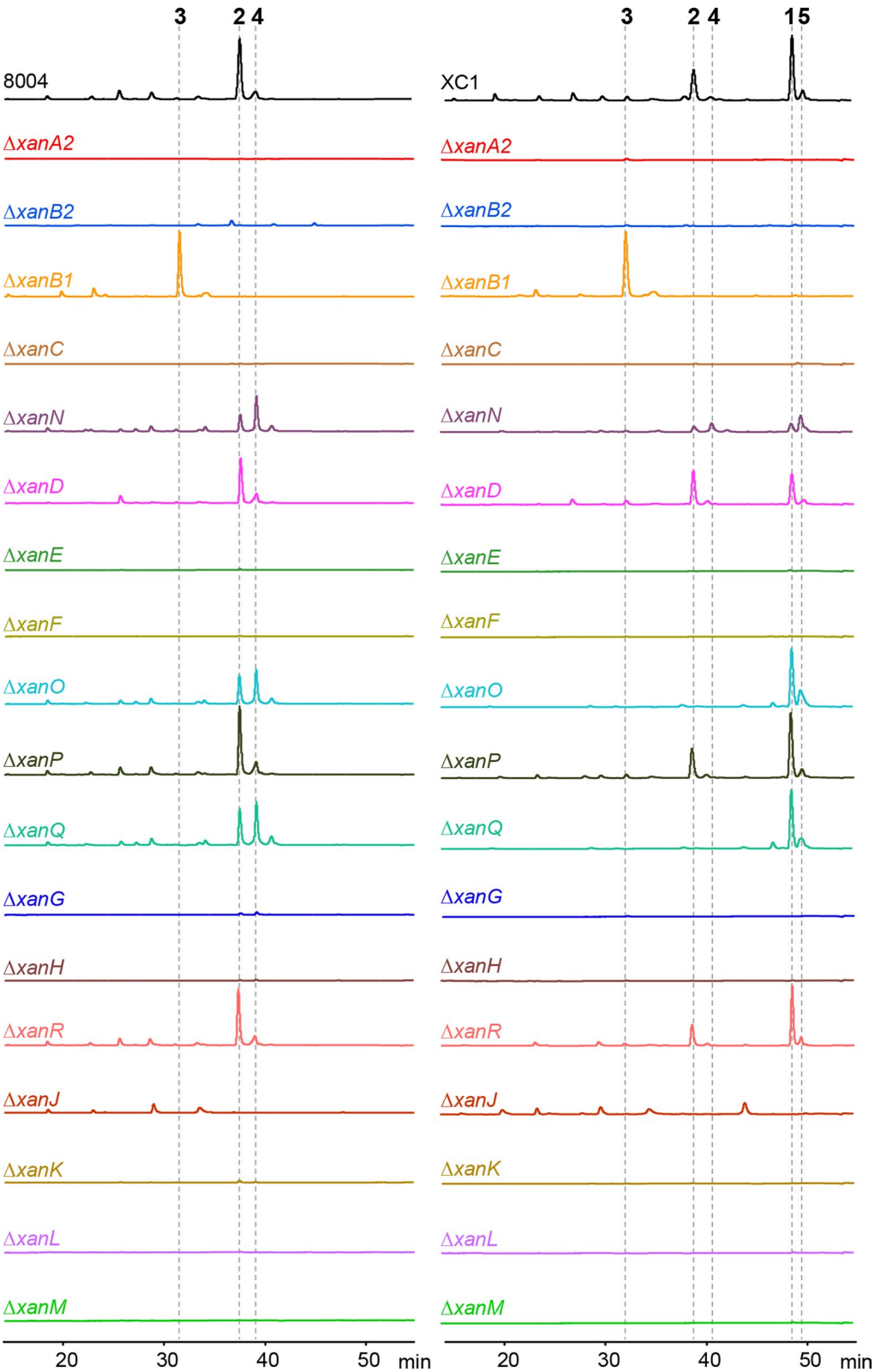

Fig. 6 HPLC analysis of MEAP profiles in *Xcc* strains 8004 (left column), XC1 (right column), and the derived *xan* deletion mutants. 1: methylated, di-brominated MEAP-1 ($C_{25}H_{24}Br_2O_3$); 2: di-brominated MEAP-2 ($C_{24}H_{22}Br_2O_3$); 3: mono-brominated MEAP-3 ($C_{24}H_{23}BrO_3$); 4: tri-brominated MEAP-4 ($C_{24}H_{21}Br_3O_3$); 5: methylated, tri-brominated MEAP-5 ($C_{25}H_{23}Br_3O_3$)

Table 3 Summary of *xan* gene functions, mutant colony colors, MEAP profiles, and the proposed key steps in MEAP biosynthesis in *Xcc*

Gene Name	Functions	Mutant colony color	Mutant MEAP profile	Roles in xanthomonadin biosynthesis
xanA2 (*Xcc4015*)	3-HBA-AMP ligase	White	Non	I
xanB2 (*Xcc4014*)	3-HBA and 4-HBA synthase	White	Non	I
xanB1 (*Xcc4013*)	Flavin-dependent brominase	Yellow	MEAP-3	IV
xanC (*Xcc4012*)	Acyl carrier protein (ACP)	White	Non	I
xanN (*Xcc4011*)	Membrane protein	Yellow	MEAP-1, 2, 4, 5 or MEAP-2, 4	V, bromination-related
xanD (*Xcc4010*)	Membrane protein, 1-acyl-*sn*-glycerol-3-phosphate acyltransferase	Yellow	MEAP-1, 2 or MEAP-2	III
xanE (*Xcc4009*)	β-hydroxy-ACP dehydratase	White	Non	II
xanF (*Xcc4008*)	Lipid Acyltransferase (AT)	White	Non	III
xanO (*Xcc4007*)	Outer membrane lipoprotein carrier protein LolA-like	Yellow	MEAP-1, 5 or MEAP-2, 4	V, bromination-related
xanP (*Xcc4006*)	Unknown	Yellow	MEAP-1, 2 or MEAP-2	
xanQ (*Xcc4005*)	Xanthomonadin exporter	Yellow	MEAP-1, 5 or MEAP-2, 4	V, bromination-related
xanG (*Xcc4004*)	β-hydroxy-ACP dehydratase	White	Non	II
xanH (*Xcc4003*)	3-oxoacyl-ACP ketoreductase (KR)	White	Non	II
xanI (*Xcc4002*)	AAA + family ATPase	?	nd	
xanR	Unknown	Yellow	MEAP-1, 2 or MEAP-2	
xanJ (*Xcc4001*)	Flavin-dependent brominase	Light yellow	Non	II, IV
xanK (*Xcc4000*)	Glycosyltransferase	White	Non	II
xanL (*Xcc3999*)	β-ketoacyl-ACP synthase chain length factor (CLF)	White	Non	II
xanM (*Xcc3998*)	β-Ketoacyl-ACP synthase (KS)	White	Non	II

I 3-HBA biosynthesis and activation, II biosynthesis of aryl polyene via polyketide synthesis pathway, III Esterification of the aryl polyene to glycerol, IV Bromination of MEAP, V Export of xanthomonadins to the outer membrane

Sequence analysis indicates that *xanD* encodes a membrane protein homologous to 1-acyl-*sn*-glycerol-3-phosphate acyltransferase, which catalyzes the esterification of the acyl chain of acyl-coenzyme A to the *sn*1 position of glycerol-3-phosphate to form lysophosphatidic acid (Johnson et al. 2023). The *xanD* deletion mutants displayed a yellow color which was similar to the wild-type *Xcc* strains 8004 and XC1 (Table 3). However, the deletion of *xanD* significantly decreased xanthomonadin yield by 29% in 8004 and 31% in XC1 (Fig. 7b, c). HPLC analysis showed that the deletion of *xanD* in 8004 significantly decreased the level of MEAP-2. This could be complemented by overexpression of *xanD* (Fig. 7d). Deletion of *xanD* in XC1 significantly decreased the level of methylated MEAP-1. The decreased xanthomonadin yield of MEAP-1 in the strain XC1-Δ*xanD* could be complemented by overexpression of *xanD* (Fig. 7e). These results suggest that XanD may be partially associated with xanthomonadin biosynthesis.

Sequence analysis indicates that *xanJ* (Xcc4001 in ATCC33913) encodes a 541-aa flavin-dependent halogenase. Deletion of *xanJ* significantly reduced xanthomonadin yield by 46% in XC1 and 51% in 8004 (Zheng et al. 2023). The resultant Δ*xanJ* mutant strains displayed a pale-yellow color on YEBB medium (Table 3). HPLC analysis revealed that neither the dominant MEAP-1 nor the dominant MEAP-2 was present in XC1 or 8004 Δ*xanJ* mutant strains, although a few minor uncharacterized MEAPs were observed (Fig. 6). Overexpression of *xanJ* in Δ*xanJ* mutant strains restored MEAP production

(See figure on next page.)

Fig. 7 Xanthomonadin yield and MEAP analysis in *Xcc* mutant strains with tri-brominated MEAPs. **a** Domain organization of XanD, XanN, XanO, and XanQ. TM: transmembrane domain; PlsC: glycerolphosphate acyltransferase; LolA: outer-membrane lipoprotein carrier protein; RPT 1: internal repeat 1; MMPL: mycobacterial membrane protein large. **b** Xanthomonadin yield (indicated by OD_{441}) in the wild-type strain 8004, Δ*xanD*, Δ*xanN*, Δ*xanO*, and Δ*xanQ* mutant strains, and derived complementation strains. **c** Xanthomonadin yield (indicated by OD_{441}) in the wild-type strain XC1, Δ*xanD*, Δ*xanN*, Δ*xanO*, and Δ*xanQ* mutant strains and derived complementation strains. **d** HPLC analysis of the MEAP patterns in the 8004-derived strains. **e** HPLC analysis of the MEAP patterns in the XC1-derived strains

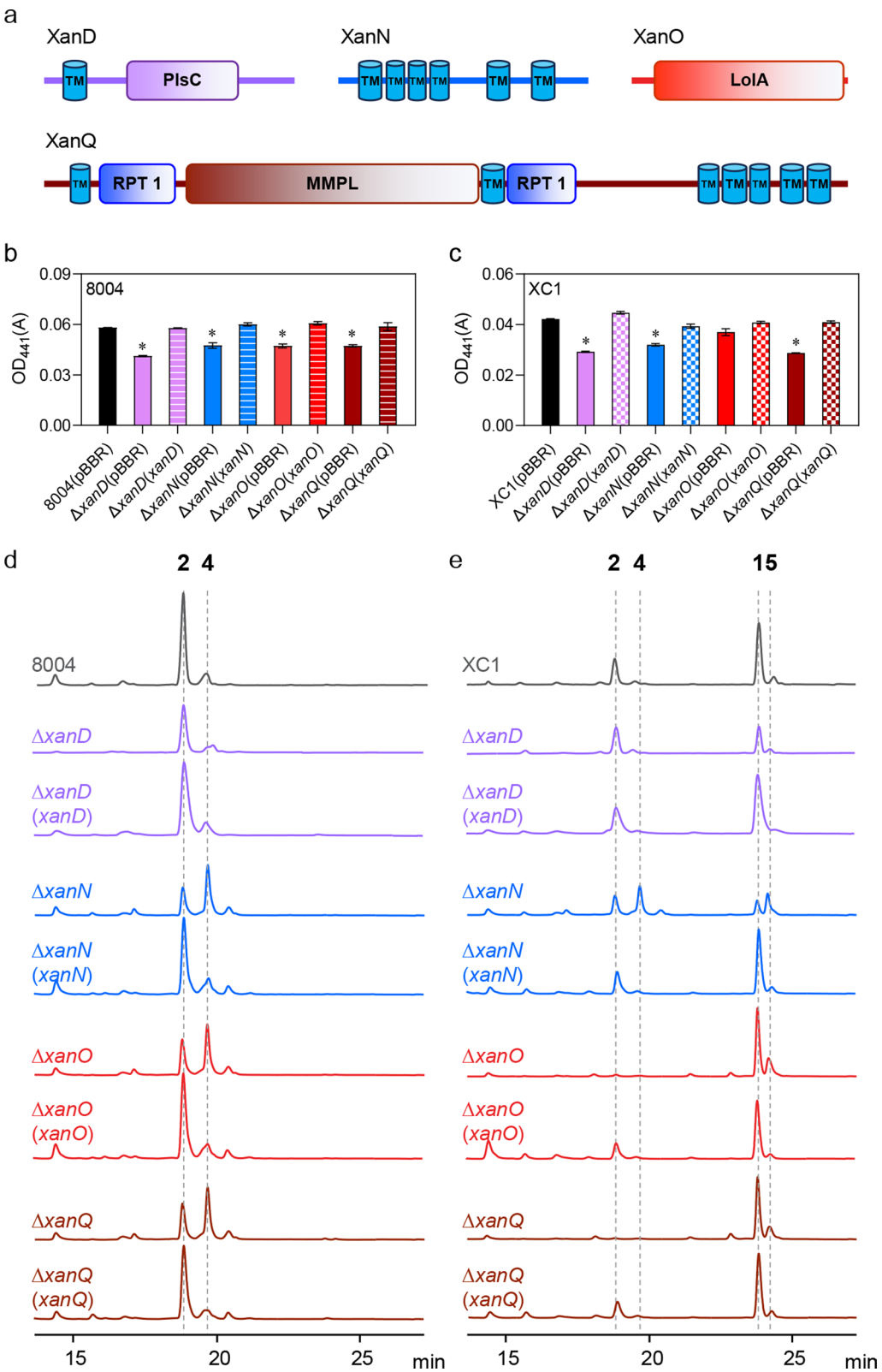

Fig. 7 (See legend on previous page.)

to that of the wild-type strains (Zheng et al. 2023). These results suggest that XanJ is involved in MEAP biosynthesis in *Xcc*. The brominase activity of XanJ remains to be determined.

xanN encodes a 248-aa functionally uncharacterized membrane protein (Fig. 7a); *xanN* deletion significantly decreased xanthomonadin yield by 19% in 8004 and 26% in XC1 (Fig. 7b, c). HPLC analysis revealed that *xanN* deletion significantly decreased the level of MEAP-2 and resulted in an accumulation of a new MEAP (named MEAP-4) in strain 8004 (Fig. 7d). In XC1, deletion of *xanN* decreased the level of both MEAP-1 and -2 and led to the accumulation of MEAP-4 and another new MEAP (named MEAP-5) (Fig. 7e). The decreased xanthomonadin yield and accumulation of MEAP-4 and/or MEAP-5 in the *xanN* deletion strains of 8004 and XC1 could be reversed by overexpression of *xanN* (Fig. 7d, e).

UPLC-Q-TOF–MS analysis further identified the presence of MEAPs -4 and -5 in the Δ*xanN* strains (Fig. 8a, b). In MEAP-4, the relative abundance ratio of the observed *m/z* 594.9086, 596.9074, 598.9055, and 600.9039 was 1:3:3:1, indicating that MEAP-4 contains three bromines. MEAP-4 may therefore be a non-methylated tri-brominated MEAP with a molecular formula of $C_{24}H_{21}Br_3O_3$ (Fig. 8c). Similarly, UPLC-Q-TOF–MS analysis suggested that MEAP-5 is a methylated tri-brominated MEAP with a molecular formula of $C_{25}H_{23}Br_3O_3$ (Fig. 8d). These results suggest that XanN is associated with xanthomonadin biosynthesis and bromination in *Xcc*.

xanO encodes a protein homologous to the outer membrane lipoprotein carrier protein LolA (Fig. 7a). Deletion of *xanO* significantly decreased xanthomonadin yield by 19% in 8004 and 14% in XC1 (Fig. 7b, c). HPLC analysis revealed that *xanO* deletion significantly decreased the level of MEAP-2 and resulted in an accumulation of MEAP-4 in strain 8004 (Fig. 7d). With XC1, *xanO* deletion significantly decreased the levels of MEAP-1 and -2 and resulted in an accumulation of MEAP-5 (Fig. 7e). The presence of MEAP-4 and -5 was later confirmed with UPLC-Q-TOF–MS (Fig. 8a). The decreased xanthomonadin yield and the accumulation of MEAP-4 or MEAP-5 in Δ*xanO* strains could be reversed by overexpression of *xanO* (Figs. 7b, c, 8a). These results suggest that XanO is probably associated with xanthomonadin biosynthesis and bromination in *Xcc*.

xanQ encodes a 788-aa protein homologous to the mycobacterial membrane protein large family transporters, which function in the export of lipid components across the cell envelope (Fig. 7a). Deletion of *xanQ* significantly decreased xanthomonadin yield by 19% in 8004 and 33% in XC1 (Fig. 7b, c). HPLC analysis revealed that the MEAP profiles of Δ*xanQ* strains are similar to that of Δ*xanO* in both 8004 and XC1 (Fig. 7d, e). UPLC-Q-TOF–MS analysis identified the presence of MEAP-4 in strain 8004-Δ*xanQ* and MEAP-5 in strain XC1-Δ*xanQ* (Fig. 8a). The decreased xanthomonadin yield and accumulation of MEAP-4 or MEAP-5 in the Δ*xanQ* mutant strains could be complemented by overexpression of *xanQ* (Figs. 7b, c, 8a). Thus, XanQ is likely associated with xanthomonadin biosynthesis and bromination in *Xcc*.

xanR and *xanP* each encode a functionally unknown protein. Deletion of *xanR* and *xanP* had no effect on MEAP biosynthesis in 8004 and XC1 (Fig. 6), suggesting that they are not essential for xanthomonadin biosynthesis. Consistent with this finding, both *xanR* and *xanP* are not present in the *xan* clusters of the strains *Xoo*, *Xoc*, and *Xal* (Fig. 5).

Discussion

As one subgroup of the widely distributed aryl polyene (APE) family of metabolites, xanthomonadins are found in plant pathogens such as *Xanthomonas*, *Xylella fastidiosa*, and *Pseudoxanthomonas* spp. However, they are also produced by a diversity of environmental bacterial species including *Rhodanobacter* spp., *Frateria aurantia*, *Herminiimonas arsenicoxydans*, *Variovorax paradoxus*, *Dechloromonas aromatica* RCB, and *Lysobacter enzymogenes* (Wang et al. 2013; Zhou et al. 2013; He et al. 2020). The structure, biosynthesis, and biological roles of xanthomonadins have long attracted researchers' attention. However, due to their complex phospholipid-like structures, xanthomonadins have not yet been fully purified and structurally characterized. Only the aryl polyene of xanthomonadin was structurally characterized in *X. arboricola* pv. *juglandis* (Andrewes et al. 1976). In this study, we established an improved method to prepare MEAPs and analyzed the MEAP patterns of 24 *Xanthomonas* strains by HPLC and MS. Our results revealed a diversity of MEAP patterns among the 24 *Xanthomonas* strains. Of the 3 dominant MEAPs, MEAP-1 corresponded to the previously characterized isobutyl ester of aryl polyene in *X. arboricola* pv. *juglandis*, while MEAP-2 and MEAP-3 represent two newly characterized aryl polyenes. All of these dominant MEAPs contain a conserved aryl group and a polyene chain but differ in bromination and methylation. Based on which MEAPs were dominant, the *Xanthomonas* strains could be grouped into three categories. Category-I is distinguished by the presence of a dominant methylated and di-brominated MEAP-1, represented by the *Xcc* strains XC1, CN01, CN04, CN07, CN11, CN17, CN18, and all *Xoc* strains (Table 2). Category-II members have a dominant non-methylated, di-brominated MEAP-2, represented by *Xcc* strains ATCC33913, 8004, CN05, CN09, CN15, and all *Xoo* and *Xal* strains (Table 2). Category-III consists of both *Xcci* strains and is distinguished

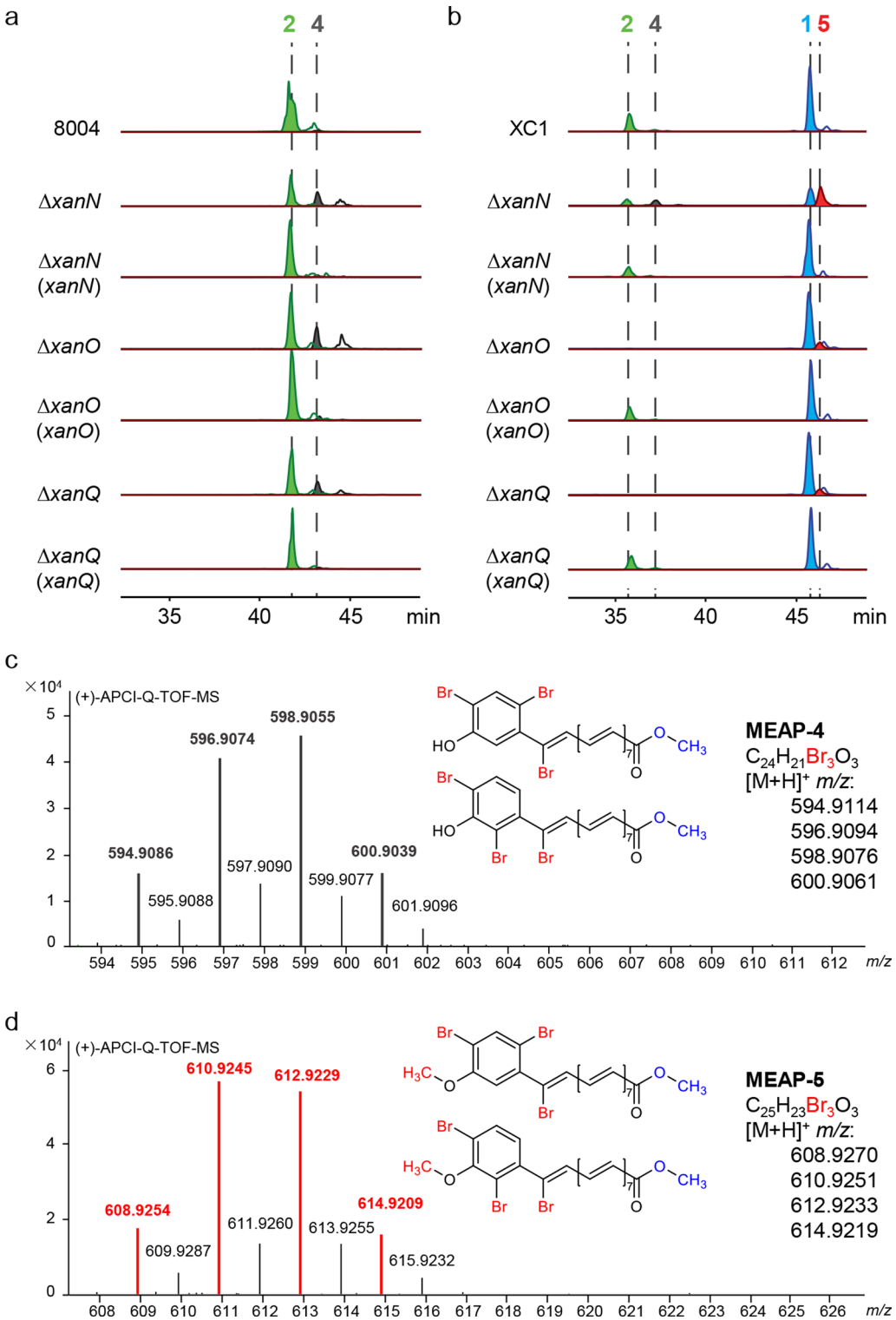

Fig. 8 UPLC-Q-TOF–MS analysis of the tri-brominated MEAPs -4 and -5 in *Xcc*-derived mutant strains Δ*xanN*, Δ*xanO,* and Δ*xanQ*. **a** Extracted ion chromatograms (EICs) corresponding to MEAP-2 ($[M+H]^+ = 517.0012$) and -4 ($[M+H]^+ = 594.9086$) in 8004 and the derived mutant strains. **b** EICs corresponding to MEAP-1 ($[M+H]^+ = 531.0178$), -2, -4, and -5 ($[M+H].^+ = 608.9254$) in XC1 and the derived mutant strains. **c** Q-TOF–MS analysis of MEAP-4. **d** Q-TOF–MS analysis of MEAP-5

by co-dominant MEAPs -1, -2, and -3 (Table 2). These findings also indicate that the MEAP patterns of these strains do not seem to be closely related to their respective host environment. This is probably due to the genome variation of *Xanthomonas* strains or the artificial YEBB rich medium used in this study. Further analysis of the in vivo MEAP pattern in all the other *Xanthomonas* strains might help to elucidate the relationship between the MEAP pattern and the host environment.

For the first time, this study shows that *Xcc* strains can be divided into two sub-groups based on MEAP profiles. It is interesting to speculate that this division may reflect two different pigment strategies the pathogen may use for a successful interaction with its host plant, and this may explain the observation that *Xoo* and *Xoc* strains are also in different categories (Table 2). Xanthomonadin production has been used as a chemotaxonomic marker for *Xanthomonas* strains (He et al. 2020). Whether the MEAP profiles can be used for *Xanthomonas* classification deserves further investigation. In the future, more *Xanthomonas* strains and xanthomonadin-producing strains of *Xylella*, *Pseudoxanthomonas*, and *Lysobacter* should be analyzed for their MEAP patterns. Such analysis could generate a greater diversity of MEAP patterns and provide more clues for further investigation of biosynthetic mechanisms.

Methylation is a universal process that covalently adds methyl groups to a variety of biomacromolecules (Menezo et al. 2020). S-adenosyl methionine (SAM) is the universal methyl group donor, and methylation is carried out by methyltransferase enzymes. The molecular substrates of these methyltransferases include nucleic acids, proteins, lipids, and secondary metabolites (Mattei et al. 2022). Although no methyltransferase-encoding gene was found in the *xan* cluster (Fig. 5), a methylated aryl polyene was identified in *X. arboricola* pv. *juglandis* by Andrewes et al. (1976), and we identified methylated MEAP-1 in 7 *Xcc* strains (XC1, CN01, CN04, CN07, CN11, CN17, CN18), 3 *Xoc* strains, and 2 *Xcci* strains (Fig. 2). A low level of MEAP-1 was also found in all 5 *Xoo* strains. However, non-methylated MEAP-2 and MEAP-3 were found in the 5 *Xcc* and 2 *Xal* strains. Considering the high conservation of the *xan* gene cluster in *Xanthomonas*, these results suggest that an uncharacterized methyltransferase "X" exists in the *Xanthomonas* genome but outside the *xan* cluster. The activity of X is probably strain-specific in *Xcc*. Since the genome sequences of all these representative *Xanthomonas* strains are available, future comparative genome analysis might identify the putative X gene responsible for xanthomonadin methylation.

The molecular mechanisms of xanthomonadin bromination are not well understood. Previous work showed that the aryl polyene of *X. arboricola* pv. *juglandis* contains two bromine modifications, which suggested the evolution of *Xanthomonas* from marine bacteria (Andrewes et al. 1976; Starr et al. 1977). Consistent with these previous findings, the study identified di-brominated MEAP-1 and MEAP-2 in *Xcc*, *Xoo*, *Xoc*, and *Xal* strains. Interestingly, the present study also identified the mono-brominated MEAP-3 in the citrus canker causal agent *Xcci* (Fig. 2). To explore the genes responsible for bromination, we did gene deletion and MEAP profile analysis in *Xcc* strains 8004 and XC1. Our preliminary results suggest that the putative flavin-dependent halogenase XanB1 is responsible for the partial bromination of the di-brominated MEAPs -1 and -2 since the deletion of *xanB1* in both strains resulted in the accumulation of the mono-brominated MEAP-3 (Fig. 6). The detailed genetic and biochemical analysis of XanB1 in xanthomonadin bromination is still underway. Our previous results showed that deletion of *xanJ*, encoding a 541-aa halogenase, significantly decreased xanthomonadin yield (Zheng et al. 2023). The present study further showed that deletion of *xanJ* disrupted the production of MEAP-1, MEAP-2, and MEAP-3 and resulted in the accumulation of several minor uncharacterized MEAPs in *Xcc* strains (Fig. 6). Thus, the XanJ-dependent bromination is also involved in xanthomonadin biosynthesis. Similar biosynthetic mechanisms have been reported in several bacterial species. A conserved gene cluster *bmp* is responsible for synthesizing polybrominated diphenyl ethers (PBDEs). In the PBDE biosynthetic pathway, the flavin-dependent brominase Bmp2 is responsible for the bromination of pyrrolyl-S-Bmp1 (ACP) to tribromopyrrolyl-S-Bmp1 (ACP). The resultant product is subsequently used as a substrate for PBDE synthesis (Agarwal et al. 2014). With the epiphytic cyanobacterium *Aetokthonos hydrillicola*, the polybromophenol-based toxins are synthesized via the products of a gene cluster *aetABCDEF*. The halogenase AetF brominates L-tryptophan to form 5,7-dibromo L-tryptophan, which is further used for the biosynthesis of the cyanobacterial toxin (Adak et al. 2022). The exact bromination positions and the details of XanB1 and XanJ involvement in *Xcc* xanthomonadin biosynthesis are under investigation.

Furthermore, the present study identified the accumulation of tri-brominated MEAP-4 and MEAP-5 and a decreased level of di-brominated MEAP-1 or MEAP-2 in the mutant strains Δ*xanN*, Δ*xanO*, and Δ*xanQ* (Figs. 6, 7). Our unpublished data showed that the *xanN-*, *xanO-*, or *xanQ*-dependent tri-bromination was only observed in the presence of *xanB1*. These results suggest that *Xcc* can regulate xanthomonadin bromination levels. Since sequence analysis indicates that XanN, XanO, and XanQ are not likely to be brominases, these proteins probably

interact with the brominases XanB1 to control the bromination level. The molecular mechanisms underlying bromination level control deserve further investigation.

Xanthomonas bacteria are plant pathogens that multiply within their host plants. However, almost all the xanthomonadin-associated research has been conducted with artificial culture. Very little attention has been paid to the xanthomonadins produced *in planta* by *Xanthomonas* during infection of their host plants. In this study, we collected the bacterial oozes on *Xoo*-infected leaves and conducted a MEAP analysis. The dominant pigment was MEAP-2, and the MEAP profile was very similar to that of the causal strain grown in YEBB medium (Fig. 4). To our knowledge, this is the first characterization of xanthomonadin production during *Xanthomonas* pathogenesis.

Why is there such a diversity of xanthomonadins (MEAPs) produced by *Xanthomonas*? Although we have found that the MEAP profiles of *Xoo*-infected rice leaves and *Xoo* grown in YEBB artificial medium are almost identical, it cannot be assumed that the MEAP profiles observed when *Xanthomonas* strains are grown in vitro are necessarily the same as those occur *in planta*. Collectively, the 27 analyzed *Xanthomonas* strains produced at least three major MEAP variants, and when particular *xan* genes were deleted/inactivated, additional variants occurred. Although most strains produced only a subset of these MEAP variants in vitro, it is possible that each strain can produce any of these variants in vivo depending on environmental conditions. Previous work has shown that xanthomonadin pigments are important for multiple reasons, including virulence (antioxidant activity), epiphytic survival (protection against photobiological damage), and infection via the leaf hydathodes (reason unknown) (He et al. 2020). Different xanthomonadin (MEAP) variants may have different efficacies with regard to antioxidant activity, protection against photobiological damage, or other capabilities. Thus, future research may show that *Xanthomonas* pathogens can selectively produce the xanthomonadin variant most suited to the particular life phase they find themselves in.

Conclusions

In conclusion, the present study provides insights into the MEAP diversity of *Xanthomonas* strains and the roles of *xan* genes in xanthomonadin biosynthesis. Based on the present study and previous findings, the biosynthesis of xanthomonadin involves the following five key steps: (I) Biosynthesis of the starter 3-HBA-S-ACP; (II) Biosynthesis of aryl polyene via a type II polyketide synthase biosynthetic pathway; (III) Esterification of the aryl polyene to a glycerol backbone; (IV) Bromination and methylation of MEAP; (V) Export of xanthomonadin to the outer membrane (Table 3).

Methods

Bacterial strains, plasmids, and growth conditions

All bacterial strains used in this study are listed in Table 1 and Additional file 2: Table S1. *Xanthomonas* strains were grown at 28°C in 4 types of culture media: YEBB contains yeast extract 5 g/L, tryptone 10 g/L, NaCl 5 g/L, sucrose 5 g/L, $MgSO_4{\cdot}7H_2O$ 0.5 g/L, and NaBr 1 g/L; NYGB contains yeast extract 3 g/L, peptone 5 g/L, glycerol 20 g/L, and NaBr 1 g/L; LBB contains yeast extract 5 g/L, tryptone 10 g/L, NaCl 5 g/L, and NaBr 1 g/L; XYSB contains yeast extract 0.625 g/L, K_2HPO_4 0.7 g/L, KH_2PO_4 0.2 g/L, $(NH_4)_2SO_4$ 1 g/L, $MgCl_2{\cdot}6H_2O$ 0.1 g/L, sucrose 5 g/L, and NaBr 1 g/L. When required, antibiotics were added at the following concentration: kanamycin (Kan) 50 μg/mL; rifampicin (Rif) 25 μg/mL. *Escherichia coli* strains were cultivated in LB medium at 37°C. Bacterial growth was assessed by measuring optical density at a wavelength of 600 nm (OD_{600}).

Growth and xanthomonadin yield of 24 Xanthomonas strains

Bacterial growth was monitored on a Bioscreen C FP-1100-C Automated Growth Curve Analysis System (Oy Growth Curves Ab Ltd, Finland). Briefly, *Xanthomonas* strains were individually inoculated into wells of Honeycomb® 10×10-well microplates, each well containing 300 μL of culture media. Strains were allowed to grow under continuous shaking, and the OD_{600} was recorded at 15-min intervals over the course of 2 d. A non-linear fitting curve was generated using the GraphPad Prism (version 8.0.1).

For quantitative measurement of xanthomonadin yield, cells of *Xanthomonas* strains were collected via centrifugation (2400 *g*, 10 min) and then extracted with 200 μL of methanol for 10 min with shaking. After another round of centrifugation (2400 *g*, 10 min), the supernatant of each well was transferred into a clear 96-well microplate. Absorbance at a wavelength of 441 nm was measured with a Spark® multimode microplate reader (Tecan Trading AG, Switzerland).

Gene deletion and complementation

Xcc mutant strains were generated following the method described by Song et al. (2022). Briefly, two ~ 500 bp DNA fragments corresponding to the upstream and downstream regions of the target gene were amplified by PCR using the primers listed in Additional file 2: Table S2. The fragments were fused by PCR, and then cloned into the vector pK18mobsacB to obtain a recombinant plasmid using a ClonExpress II One Step Cloning Kit (Vazyme, China). Recombinant plasmids were then transformed

into *Xcc* through *E. coli* S17-1(λpir)-mediated mating. Kan and Rif resistant colonies were subsequently selected on NYG agar media containing Kan and Rif. The colonies were then plated on NYG agar plates with Rif and 50 g/L sucrose. Mutant colonies were verified by PCR and DNA sequencing using the primers listed in Additional file 2: Table S2. For complementation analysis, the target gene was PCR amplified and cloned into the multiple cloning site of the expression plasmid pBBR1MCS-2. These constructed plasmids were then transferred to *Xcc* strains by triparental mating. All plasmids and primers used in the cloning process are listed in Additional file 2: Table S2 and Table S3.

Preparation of xanthomonadin MEAPs

The xanthomonadin-derived MEAPs were prepared following a previously described method (Grammbitter et al. 2019). Briefly, *Xanthomonas* strains were grown in 50 mL of YEBB liquid medium for 24 h at 28°C. The culture was then centrifuged at 9600 *g* for 10 min, and the resultant pellets were extracted in 30 mL methanol/dichloromethane (1:2, v/v) with shaking at room temperature for 10 min. Cell debris was removed by centrifugation, and the crude extract was then treated with 15 mL of 0.5 M KOH for 1 h at room temperature with stirring. After neutralization with 2 M H_2SO_4, the organic layer was first washed with saturated sodium chloride and then with deionized water. The MEAP extract was finally dried and dissolved in 1 mL of methanol/dichloromethane (1:1, v/v) for further HPLC or LC–MS analysis.

HPLC and UPLC-Q-TOF–MS analysis of MEAPs

A 10 μL aliquot of MEAP extract was loaded onto a C18 reverse-phase analytical column (Agilent Eclipse XDB-C18, 5 μm, 4.6×150 mm) on an Agilent 1260 Infinity HPLC. The column was then eluted by a gradient of H_2O (Solvent A) and acetonitrile (Solvent B) (0–5 min 5% B, 5–5.1 min 5–60% B, 5.1–50 min 60–100% B, 50–55 min 100% B, 55–55.1 min 100–5% B, 55.1–60 min 5% B) at a flow rate of 1 mL/min. The elution profile was monitored by following the absorbance at 441 nm.

UPLC-Q-TOF–MS analysis was performed on an Agilent 1290 Infinity II UPLC system in tandem with a G6545B Accurate Mass Q-TOF mass spectrometer. Spectra were recorded in positive mode from the Atmospheric Pressure Chemical Ionization ($APCI^+$) source. The column was eluted by a gradient of H_2O (Solvent A) and acetonitrile (Solvent B): (0–5 min 5% B, 5–5.1 min 5–60% B, 5.1–50 min 60–100% B, 50–55 min 100% B, 55–55.1 min 100–5% B, 55.1–60 min 5% B) at a flow rate of 0.6 mL/min. Data were processed using MassHunter Workstation Software (version B.08.00).

Collection of dry Xoo ooze on rice leaf blade and MEAP analysis

Droplets of *Xoo* ooze can be observed early in the morning at the edges of leaf blades with no visible lesions (Mansfield et al. 2012). The droplets accumulate and dry to form granular yellow oozes attached to the surface of rice leaf blades. Each ooze consists of *Xoo* cells, extracellular polysaccharides and other components, and ranges from 0.5–2.0 mm in size. These granular oozes were carefully collected with forceps from the infected leaves of rice (*Oryza sativa* Huazheyou-1) at Dongyang, Zhejiang. Five mg of *Xoo* ooze was ground and dissolved in 500 μL of water. After centrifuging at 9600 *g* for 10 min, the resulting cell pellet was resuspended and extracted with 3 mL of methanol/dichloromethane (1:2, v/v). The resultant extract was then esterified and purified for MEAP analysis by HPLC and UPLC-Q-TOF–MS following the above-mentioned method.

Bioinformatic analysis and data processing

DNA sequences of the *xan* cluster were downloaded from the microbial genome database of National Center of Biotechnology Information at https://www.ncbi.nlm.nih.gov/. Multiple DNA or amino acid sequence alignments were conducted using MEGA 11 based on the ClustalW algorithm. Protein domain organization prediction was performed using the SMART online tool at http://smart.embl-heidelberg.de/. Cluster alignment was performed with Clinker (Gilchrist and Chooi 2021).

Abbreviations

3-HBA-S-ACP	3-Hydroxybenzoic acid-S-acyl carrier protein
LBB	Luria broth with bromide
MEAP	Methyl ester of aryl polyene
NYGB	Nutrient yeast glycerol with bromide
PBDE	Polybrominated diphenyl ethers
SAM	S-adenosyl methionine
Xal	*Xanthomonas albilineans*
Xcc	*Xanthomonas campestris* pv. *campestris*
Xcci	*Xanthomonas citri* pv. *citri*
Xoc	*Xanthomonas oryzae* pv. *oryzicola*
Xoo	*Xanthomonas oryzae* pv. *oryzae*
XYSB	Xylem-Yeast Extract with bromide
YEBB	Yeast extract beef with bromide

Supplementary Information

The online version contains supplementary material available at https://doi.org/10.1186/s42483-025-00314-8.

Additional file1: Figure S1. Deletion of genes encoded in the *xan* biosynthetic cluster had no significant effect on the growth of *Xcc* strains.

Additional file2: Table S1. *E. coli* and *Xanthomonas* mutant strains used in this study. **Table S2.** Bacterial plasmids used in this study. **Table S3.** DNA primers used in this study. Overhangs are underlined.

Acknowledgements
We thank Prof. Gongyou Chen and Prof. Hui-Li Zhang for providing the *Xcci* and *Xal* strains.

Author contributions
WH, ZZ, and YH contributed to the concept and design of the study. Material preparation, data collection, and analysis were jointly completed by WH, ZZ, and YH. BC, WH, and YH completed additional experiments on MEAP production *in planta*. The manuscript was co-written and edited by YH, WH, and AP. All authors read and approved the final manuscript.

Funding
This work was financially supported by research grants from the Natural Science Foundation of China (31972231 and 32172355).

Availability of data and materials
Not applicable.

Declarations

Ethics approval and consent to participate
Not applicable.

Consent for publication
Not applicable.

Competing interests
The authors declare no competing interests.

Author details
[1]State Key Laboratory of Microbial Metabolism, Joint International Research Laboratory of Metabolic and Developmental Sciences, School of Life Sciences and Biotechnology, Shanghai Jiao Tong University, Shanghai 200240, China. [2]Institute of Maize and Featured Dryland Crops, Zhejiang Academy of Agriculture Sciences, Dongyang 322100, Zhejiang, China. [3]Department of Entomology, Plant Pathology and Nematology, University of Idaho, Moscow, ID 83844, USA.

Received: 4 September 2024 Accepted: 13 January 2025
Published online: 29 April 2025

References

Adak S, Lukowski AL, Schäfer RJB, Moore BS. From tryptophan to toxin: nature's convergent biosynthetic strategy to aetokthonotoxin. J Am Chem Soc. 2022;144:2861–6.
Agarwal V, El Gamal AA, Yamanaka K, Poth D, Kersten RD, Schorn M, et al. Biosynthesis of polybrominated aromatic organic compounds by marine bacteria. Nat Chem Biol. 2014;10:640–7.
An SQ, Potnis N, Dow M, Vorhölter F-J, He YQ, Becker A, et al. Mechanistic insights into host adaptation, virulence and epidemiology of the phytopathogen *Xanthomonas*. FEMS Microbiol Rev. 2020;44:1–32.
Andrewes AG, Jenkins CL, Starr MP, Shepherd J, Hope H. Structure of xanthomonadin I, a novel dibrominated aryl-polyene pigment produced by the bacterium *Xanthomonas juglandis*. Tetrahedron Lett. 1976;45:4023–4.
Aririatu LE, Kester AS. Isolation and characterization of the pigment esters of *Xanthomonas juglandis* (*campestris*). Microbiology. 1985;131:2047–52.
Cao XQ, Wang JY, Zhou L, Chen B, Jin Y, He YW. Biosynthesis of the yellow xanthomonadin pigments involves an ATP-dependent 3-hydroxybenzoic acid: acyl carrier protein ligase and an unusual type II polyketide synthase pathway. Mol Microbiol. 2018;110:16–32.
Gilchrist CL, Chooi YH. Clinker & clustermap. js: Automatic generation of gene cluster comparison figures. Bioinformatics. 2021;37(16):2473–5.
Goel AK, Rajagopal L, Nagesh N, Sonti RV. Genetic locus encoding functions involved in biosynthesis and outer membrane localization of xanthomonadin in *Xanthomonas oryzae* pv. *oryzae*. J Bacteriol. 2002;184:3539–48.
Grammbitter GLC, Schmalhofer M, Karimi K, Shi YM, Schöner TA, Tobias NJ, et al. An uncommon type II PKS catalyzes biosynthesis of aryl polyene pigments. J Am Chem Soc. 2019;141:16615–23.
Hayward AC. The hosts of *Xanthomonas*. In: Swings JG, Civerolo EL, editors. Xanthomonas. Dordrecht: Springer Netherlands; 1993. p. 1–119. https://doi.org/10.1007/978-94-011-1526-1_1.
He YW, Zhang LH. Quorum sensing and virulence regulation in *Xanthomonas campestris*. FEMS Microbiol Rev. 2008;32:842–57.
He YW, Wu J, Zhou L, Yang F, He YQ, Jiang BL, et al. *Xanthomonas campestris* diffusible factor is 3-hydroxybenzoic acid and is associated with xanthomonadin biosynthesis, cell viability, antioxidant activity, and systemic invasion. Mol Plant-Microbe Interact. 2011;24:948–57.
He YW, Cao XQ, Poplawsky AR. Chemical structure, biological roles, biosynthesis and regulation of the yellow xanthomonadin pigments in the phytopathogenic genus *Xanthomonas*. Mol Plant-Microbe Interact. 2020;33:705–14.
Johnson ZL, Ammirati M, Wasilko DJ, Chang JS, Noell S, Foley TL, et al. Structural basis of the acyl-transfer mechanism of human GPAT1. Nat Struct Mol Biol. 2023;30:22–30.
Leyns F, De Cleene M, Swings J-G, De Ley J. The host range of the genus *Xanthomonas*. Bot Rev. 1984;50:308–56.
Mansfield J, Genin S, Magori S, Citovsky V, Sriariyanum M, Ronald P, et al. Top 10 plant pathogenic bacteria in molecular plant pathology. Mol Plant Pathol. 2012;13:614–29.
Mattei AL, Bailly N, Meissner A. DNA methylation: a historical perspective. Trends Genet. 2022;38:676–707.
Menezo Y, Clement P, Clement A, Elder K. Methylation: an ineluctable biochemical and physiological process essential to the transmission of life. Int J Mol Sci. 2020;21:9311.
Moser R, Aktas M, Narberhaus F. Phosphatidylcholine biosynthesis in *Xanthomonas campestris* via a yeast-like acylation pathway. Mol Microbiol. 2014;91:736–50.
Niño-Liu DO, Ronald PC, Bogdanove AJ. *Xanthomonas oryzae* pathovars: model pathogens of a model crop. Mol Plant Pathol. 2006;7:303–24.
Pieretti I, Pesic A, Petras D, Royer M, Süssmuth RD, Cociancich S. What makes *Xanthomonas albilineans* unique amongst xanthomonads? Front Plant Sci. 2015;6:289.
Poplawsky AR, Kawalek MD, Schaad NW. A xanthomonadin-encoding genecluster for the identification of pathovars of *Xanthomonas campestris*. Mol Plant-Microbe Interact. 1993;6:545–52.
Poplawsky AR, Urban SC, Chun W. Biological role of xanthomonadin pigments in *Xanthomonas campestris* pv. *campestris*. Appl Environ Microbiol. 2000;66:5123–7.
Rajagopal L, Sundari CS, Balasubramanian D, Sonti RV. The bacterial pigment xanthomonadin offers protection against photodamage. FEBS Lett. 1997;415:125–8.
Song K, Chen B, Cui Y, Zhou L, Chan K-G, Zhang H-Y, He Y-W. The plant defense signal salicylic acid activates the RpfB-dependent quorum sensing signal turnover via altering the culture and cytoplasmic pH in the phytopathogen *Xanthomonas campestris*. Mbio. 2022;13(2):e0364421. https://doi.org/10.1128/mbio.03644-21.
Starr MP, Jenkins CL, Bussey LB, Andrewes AG. Chemotaxonomic significance of the xanthomonadins, novel brominated aryl-polyene pigments produced by bacteria of the genus *Xanthomonas*. Arch Microbiol. 1977;113:1–9.
Vicente JG, Holub EB. *Xanthomonas campestris* pv. *campestris* (cause of black rot of crucifers) in the genomic era is still a worldwide threat to brassica crops. Mol Plant Pathol. 2013;14:2–18.
Wang Y, Qian GL, Li YY, Wang YS, Wang YL, Wright S, et al. Biosynthetic mechanism for sunscreens of the biocontrol agent *Lysobacter enzymogenes*. PLoS ONE. 2013;8: e66633.
Williams PH. Black rot: a continuing threat to world crucifers. Plant Dis. 1980;64:736–42.
Zheng ZL, Cao XQ, Hu WD, Song K, Hao XR, Zhang HY, et al. The flavin-dependent brominase XanJ is involved in the biosynthesis of *Xanthomonas* yellow pigment xanthomonadin. Acta Phytopathol Sin. 2023;53:229–44.
Zhou L, Wang JY, Wu J, Wang J, Poplawsky A, Lin S, et al. The diffusible factor synthase XanB2 is a bifunctional chorismatase that links the shikimate pathway to ubiquinone and xanthomonadins biosynthetic pathways. Mol Microbiol. 2013;87:80–93.